MOLECULAR PHYSICS REPORTS **40** (2004) 23-33

ELECTRICAL SPIN DETECTION IN GaMnAs-BASED TUNNEL JUNCTIONS: THEORY AND EXPERIMENTS

J.-M. GEORGE[1], H. JAFFRÈS[1], R. MATTANA[1], M. ELSEN[1], F. NGUYEN VAN DAU[1], A. FERT[1], B. LÉPINE[2], A. GUIVARC'H[2], AND G. JÉZÉQUEL[2]

[1]*Unité Mixte de Physique CNRS/THALES, Domaine de Corbeville, 91404 Orsay, France and Université Paris-Sud, 91405, Orsay, France*

[2]*Equipe de Physique des Surfaces et Interfaces, Unité Mixte de Recherche CNRS-Université 6627 "PALMS" Université Rennes I, 35042 Rennes Cedex, France*

Abstract: We report on both model and experiments demonstrating how the spin injection can be probed electrically. Derivation of the conditions of spin injection and detection by considering the characteristic times involved for the spin transport is given. This yields a simple expression of the TMR as a function of the spin and carriers lifetime in the semiconductor. In a second part we will review about our structural and electrical characterisations of single GaMnAs layers and GaMnAs/AlAs/GaMnAs tunnel junctions which demonstrate the spin polarised efficiency of this magnetic semiconductor. We will then discuss our TMR experiments on double barriers junctions GaMnAs/AlAs/GaAs/AlAs/GaMnAs in the light of the theoretical results and show how these measurements constitute an electrical probe of both, the hole spin life time and the conditions to inject and detect spin polarized current in a GaAs quantum well.

1. INTRODUCTION

Introducing the spin as an additional degree of freedom in semiconductors is an important challenge for the future developments of spintronics [1-4]. Semiconductors combine the advantage of a long spin lifetime and high mobility, the flexibility of the carrier concentration together with the possibility of acting on the spin orientation through a gate voltage [5]. The long time of spin coherence in semiconductors have been demonstrated by time-resolved optical experiments and, for example, a spin lifetime reaching a fraction of μs has been evidenced in *n*-doped GaAs at low temperature [6-7]. However, the prerequisite of spin injection from a ferromagnetic conductor in most concepts of devices raises difficult problems. It has turned out that injecting spins from a ferromagnetic metal encounters difficulties related to the conductivity mismatch between metal and semiconductor [8-10] and their possible chemical incompatibility. This has driven the development of magnetic semiconductors [11-14], like $Ga_{1-x}Mn_xAs$ which is ferromagnetic up to 159 K [15], more adapted for their integration in heterostructures. Recently, successful experiments on spin injection have been achieved by injecting an electrical current from magnetic semiconductors or metals and detecting the circular polarization of the emitted light [16-23].

In this paper we will report on both model and experiments demonstrating how the spin injection can be probed electrically. The first part will be devoted to the derivation of the conditions of spin injection and detection by considering the characteristic times involved for the spin transport. This yields a simple expression of the TMR as a function of the spin and

carriers lifetime in the semiconductor. In a second part, we will report on i) the growth and characterization of the ferromagnetic semiconductor GaMnAs layers, ii) the integration of such GaMnAs layers as electrodes for tunnel junctions with AlAs barrier to probe the hole tunnel spin-polarization, iii) the hole transport in double barriers junctions in which a GaAs quantum well has been inserted in between two barriers. Such structures constitutes a complete electrical device enable to test the conditions of spin injection and spin detection in/out a GaAs QW *vs*. the resistance of tunnel junctions that circumvents the conductivity mismatch between the ferromagnetic metal and the semiconductor [9, 10].

2. SPIN INJECTION, SPIN CONSERVATION AND MAGNETORESISTANCE IN FM/SC/FM STRUCTURES

2.1. Definition and physical parameters

We consider two identical ferromagnetic (FM) contacts, *L* (left) and *R* (right), connected along the *z* direction by a semiconductor (SC) whose geometry is characterized by a channel length *t* and section *S* (relative to the contact area taken to be equal to unity).

The one dimensional (1-D) density of states (DOS) in SC and FM along *z* is noted ρ_{SC} and $\rho_{FM\pm}$ respectively where the subscript + (−) refers to up (down) spins respectively. Interfaces between FM (*L* or *R*) and SC, assumed to be identical, are characterized by *i*) a spin-dependent flux transmission, $T_\pm = T(1 \pm P)$ with the result that the tunnel polarization at the Fermi level writes $P = (T_+ - T_-)/(T_+ + T_-)$ equivalent to the Jullière definition [24] and by *ii*) the number, n_{2D}, of two-dimensional (2D) channels in SC connected to FM as appearing in the Landauer formula [25]. For a non magnetic semiconductor, these number of channels are equal for both spin populations.

From the Hamiltonian transfer approach [26], we can express for a particle *i*) its characteristic time of injection from FM (*L* or *R*) towards SC, $\tau_{FM\to SC}$, *ii)* its spin-dependent time of ejection, $\tau_\pm$, from SC into FM (*L* or *R*), and *iii)* its spin-dependent transmission ($T_\pm$). Corresponding currents ($J_{FM\pm\to SC}$) and conductivity ($G_{FM\pm\to SC}$) follows according to:

$$
\begin{aligned}
\Gamma_{FM} &= \frac{\hbar}{\tau_{FM\to SC}} = 2\pi\left|\left\langle \phi^Z_{FM}\middle|H_T\middle|\phi^Z_{SC}\right\rangle\right|^2 \rho_{SC} \\
\Gamma_{SC} &= \frac{\hbar}{\tau_\pm} = 2\pi\left|\left\langle \phi^Z_{FM}\middle|H_T\middle|\phi^Z_{SC}\right\rangle\right|^2 \rho_{FM\pm} \\
T_\pm &= (2\pi)^2\left|\left\langle \phi^Z_{FM}\middle|H_T\middle|\phi^Z_{SC}\right\rangle\right|^2 \rho_{SC}\rho_{FM\pm} \qquad (1) \\
J_{FM\pm\to SC} &= \frac{e}{\hbar}\int 2\pi\left|\left\langle \phi^Z_{FM}\middle|H_T\middle|\phi^Z_{SC}\right\rangle\right|^2 \rho_{SC}\rho_{FM\pm} d\varepsilon_{FM,SC} \\
G_{FM\pm\to SC} &= e\frac{\partial J_{FM\to SC}}{\partial \varepsilon_{FM,SC}} = \frac{e^2}{h}T_\pm
\end{aligned}
$$

ϕ_{FM} and ϕ_{SC} are the normalized one-dimensional wave functions in FM and SC connected through the interface by the transfer Hamiltonian H_T. Γ_{FM} and Γ_{SC} represents the broadening of the energy level in FM (ε_{FM}) and SC (ε_{SC}) introduced by the leak towards FM (L or R) and SC. Note that the spin-polarized current $J_{FM\pm\rightarrow SC}$ crossing each surface (L/SC or SC/R) per unit time and per unit number of 2-D channels does not depend on the propagation direction.

The escape time of a spin-polarized particle from SC into L or R, $\tau_{\pm}$, can then be expressed *vs*. the 1-D DOS, $\rho_{SC,}$ and the spin-dependent transmission at interfaces ($T_{\pm}$) according to $\tau_{\pm} = 2h\rho_{SC}/T_{\pm}$. However in a more general case, for a particle placed in the middle of the SC channel, one has to take into account that *i*) its effective transmission coefficient towards L or R, $T_{*\pm}$, must be renormalized because of the finite transmission in SC (noted T_{SC} and roughly equal λ/t where λ is the particle mean free path in SC) according to $[T_{*\pm}]^{-1}=[T_{\pm}]^{-1}+[T_{SC}]^{-1}-1$, that *ii*) the overall transmission coefficient $T_{\pm}$ must be normalized by a geometry factor S, ratio of the SC section to the contact section if they are different (*we will not consider this case from now on*) and that *iii*) the polarization P of R changes of sign when its magnetization is reversed to form the antiparallel configuration (AP). Consequently, the true escape time towards R reads $\tau_{R*\pm} = h\rho_{SC}/T_{*\varepsilon\pm}$ where $\varepsilon = +1$ in the parallel (PA) configuration whereas $\varepsilon = -1$ in the AP magnetic arrangement.

In the case of symmetric interfaces we consider there, no spin accumulation occurs in the PA state. If one introduces the characteristic time of spin-flip between up and down channels in the AP configuration, $\tau_{sf,}$ one can derive the general balance equations for both spin population in PA and AP arrangement in term of characteristic time of injection (or ejection) as:

$$\frac{1}{\tau_{\pm}} = \mu_{\pm}\left[\frac{1}{\tau_{\pm}} + \frac{1}{\tau_{\varepsilon\pm}}\right] \pm \left(\frac{1-\varepsilon}{2}\right)\frac{\mu_{+}-\mu_{-}}{\tau_{sf}} \tag{2}$$

$\mu_{\pm}$ represents here the fraction of + and – spins in SC which are ejected back to L once injected in SC instead to be transmitted into R. In the AP state, $SP = (\mu_{+} - \mu_{-})/(\mu_{+} + \mu_{-})$ represents simply the unbalance between each spin population in SC (or carrier spin-polarization). For a degenerate SC, $\mu_{\pm}$ indicates the average position of the respective + and – Fermi level in SC counted from the Fermi level in R relatively to the total potential drop applied between L and R.

In whole cases, the respective + and – spin currents flowing in R writes respectively $J_{\pm} = \mu_{\pm}/\tau_{\varepsilon\pm}$ whereas the corresponding current spin-polarization, CP, writes $(J_{+} - J_{-})/(J_{+} + J_{-})$.

2.2. Parallel state ($\varepsilon = 1$)

From Eq. 2, we have $\mu_{\pm} = 1/2$, from which we deduce the current as well as its spin polarization (CP_{PA}) in the PA configuration *vs*. characteristic times $\tau_{\pm} = h\rho_{SC}/T_{*\pm}$ according to:

$$J_{\mathrm{PA}} = J_+ + J_- \propto \frac{\mu_+}{\tau_+} + \frac{\mu_-}{\tau_-} \propto \frac{1}{2}\left[\frac{1}{\tau_+} + \frac{1}{\tau_-}\right]$$
$$CP_{\mathrm{PA}} = \frac{J_+ - J_-}{J_+ + J_-} = \frac{\dfrac{\mu_+}{\tau_+} - \dfrac{\mu_-}{\tau_-}}{\dfrac{\mu_+}{\tau_+} + \dfrac{\mu_-}{\tau_-}} = \frac{\tau_- - \tau_+}{\tau_+ + \tau_-} \tag{3}$$

Because, there is no spin accumulation in the PA state, the spin current must have only a drift component.

2.3. Antiparallel state ($\varepsilon = -1$)

From Eq. 2, we just have now $\mu_\pm = [1+\tau_{sf}/\tau_\pm]/[2 + \tau_{sf}(1/\tau_+ + 1/\tau_-)]$

$$J_{\mathrm{AP}} \propto \frac{\alpha_+}{\tau_-} + \frac{\alpha_-}{\tau_+} \propto \frac{\tau_+ + \tau_- + 2\tau_{sf}}{2\tau_+\tau_- + \tau_{sf}(\tau_+ + \tau_-)} \tag{4}$$

$$SP_{\mathrm{AP}} = \frac{\tau_{sf}(\tau_- - \tau_+)}{2\tau_-\tau_+ + \tau_{sf}(\tau_- + \tau_+)} \qquad CP_{\mathrm{AP}} = \frac{\tau_+ - \tau_-}{\tau_+ + \tau_- + 2\tau_{\mathrm{sf}}} \tag{5}$$

In the case of an infinite spin lifetime, the carrier spin-polarization SP_{AP} in SC equals the current spin polarization in the PA configuration whereas the current spin-polarization (in AP state) vanishes. In the case of infinite relaxation rate ($\tau_{sf} = 0$), no spin accumulation occurs in SC and the absolute spin-polarization of the current in *R* (negative) or in *L* (positive) is maximum equalling the one in the PA state.

2.4. Magnetoresistance

The MR = $J_{\mathrm{PA}}/J_{\mathrm{AP}} - 1$ reads now:

$$MR = \frac{[\tau_- - \tau_+]^2}{4\tau_-\tau_+} \frac{1}{1 + \dfrac{\tau_s + \tau_-}{2\tau_{\mathrm{sf}}}} \tag{6}$$

Condition for impedance matching without spin relaxation

Neglecting the spin relaxation in SC ($\tau_{\mathrm{sf}} = \infty$), the *MR* equals $(\tau_- - \tau_+)^2/4\tau_-\tau_+$ which can be expressed *vs.* the effective transmission coefficients at interfaces, $T_{*\pm}$, according to $MR = (T_{*+} - T_{*-})^2/(4T_{*+}T_{*-})$. From the upper relation $[T_{*\pm}]^{-1} = [T_\pm]^{-1} + [T_{*\mathrm{SC}}]^{-1}$ with $T_{*\mathrm{SC}} = \lambda/(t - \lambda)$, one can express the MR *vs.* the unpolarized intrinsic transmission *T* as $MR = \kappa P^2/(1 - P^2)$ with $\kappa = 1/[1 + 2T/T_{\mathrm{SC}} + (1 - P^2)(T/T_{\mathrm{SC}})^2]$. The maximum MR for symmetric double tunnel junction is then $P^2/(1 - P^2)$ that is half of TMR of single junctions.

The factor 1/2 is related to accumulation effects in the central non magnetic electrode. Starting from this optimal value, the MR decreases when $\kappa < 1$ or $T > T_{*SC}$ that is when the impedance matching is uncompleted [8, 10] for interface transparencies larger than the transmission through the SC channel. Note that this impedance mismatch is also associated with a vanishing current spin-polarization in the PA state (from Eq. 3). The introduction of tunnel junctions of small transmission $T << T_{*SC} = \lambda/(t - \lambda)$ (or high resistive enough) at the interfaces restores the current spin-polarization in PA state and consequently the *MR* [9, 10]. For a diffusive transport in SC ($t >> \lambda$), the condition $T_L < \lambda/t$ is equivalent to $T_L < \sqrt{[\tau_p/\tau_{SC}]}$ where τ_p and τ_{SC} represents respectively the momentum relaxation time (τ_p) and the characteristic time (τ_{SC}) for a particle to diffuse from the left to the right interface in SC. $1/\sqrt{[\tau_p/\tau_{SC}]}$ represents the number of reflections of a particle upon the left interface once injected in SC and before to be detected in *R* after a delay time τ_{SC}. The condition of impedance matching is then the condition for a spin to be detected in the *R* contact instead of diffusing back towards the emitter *L* (where its spin will be rapidly lost).

Condition for spin conservation with impedance matching

The second term appearing in the expression of *MR*, that is $[1 + (\tau_+ + \tau_-)/2\tau_{sf}]^{-1}$ represents a reduction factor related to the condition of spin conservation in the SC channel once the impedance matching is completed. To obtain any MR effects, the spin lifetime in SC must be larger than the mean dwell time of + and – spins in the SC channel (in the PA state). This mean dwell time is noted there τ_n and equals $(\tau_+ + \tau_-)/4$. The loss of spin memory in SC originates from to the large number of reflections against the two interfaces. This effect can be viewed as the consequence of a too large integrated ballistic path in SC compared to the spin mean free path λ_{sf} ($= v_Z \tau_{sf}$ where v_Z is the characteristic velocity along *z*). Indeed, from the upper developments, the condition for spin conservation in SC reads $T > h\rho_{SC}/\tau_{sf} \approx t/\lambda_{sf}$ or $l = t/T < \lambda_{sf}$ where *l* represents the integrated particle path in both ballistic ($t < \lambda$) or diffusive ($t > \lambda$) regimes of injection.

2.5. Conclusion

The conditions acting on the interface transparency (*T*) between FM and SC to obtain MR in FM/SC/FM junction, that is an electrical injection and detection of spins, are $t/\lambda_{sf} < T < \lambda/t$ in current-perpendicular to plane experiments (or heterostructure of constant section) and more generally $S[t/\lambda_{sf}] < T < S[\lambda/t]$ for a lateral spin transport where *S* is the ratio of the SC section to the contact section (refer to geometric effects in Ref. [10]).

3. EXPERIMENTS

3.1. GaMnAs electrodes

Samples were prepared in a RIBER 2300 molecular beam epitaxy (MBE) system equipped with an As_4 solid source. We used semi-insulating GaAs(001) wafers on which a 100 nm thick undoped GaAs buffer was first grown at high temperature using the standard conditions (substrate at 580°C, ratio between the beam equivalent pressures (BEP) of As_4 and Ga equal to about 25, growth rate of 0.3 µm/h). The growth of $Ga_{1-x}Mn_xAs$ was then initiated at 230°C on

a C4x4 As rich GaAs surface with the same rate but an As_4/Ga BEP ratio equal to 10. During and after the growth, the reflection high-energy electron diffraction (RHEED) showed a streaky pattern with a 1×2 surface reconstruction [27]. Calibration samples of 1 μm thick were made at different Mn compositions: x = 0, 0.037, 0.066, 0.071. Note that the x = 0 sample was used as a reference of the GaAs low temperature growth. The Mn composition was determined by energy dispersive analysis of X-rays (EDX) and the structural properties of the layers were studied by X-ray diffraction on a ($\omega - 2\theta$) diffractometer (CGR Theta 2000) equipped with a front curved quartz monochromator ($\lambda_{CuK\alpha 1}$ = 0.154056 nm).

Table 1. Crystallographic data of $Ga_{1-x}Mn_xAs$ samples: the lattice parameters in the directions perpendicular ($a_\perp$) and parallel ($a_{//}$) to the sample surface were determined from the measurement of the (004) and (444) plane reticular distances. The relaxed (bulk) lattice parameter (a_0) was calculated with the C_{11} and C_{12} elastic moduli of GaAs [30]

x Mn (%)	d (004) (nm)	d (444) (nm)	$a_\perp$ (nm)	$a_{//}$ (nm)	a_0 bulk (nm)
0.0	0.14141	0.08161	0.56564	0.56529	0.56549
3.7	0.14185	0.08170	0.56740	0.56538	0.56641
6.6	0.14219	0.08176	0.56878	0.56530	0.56714
7.1	0.14225	0.08178	0.56901	0.56535	0.56726

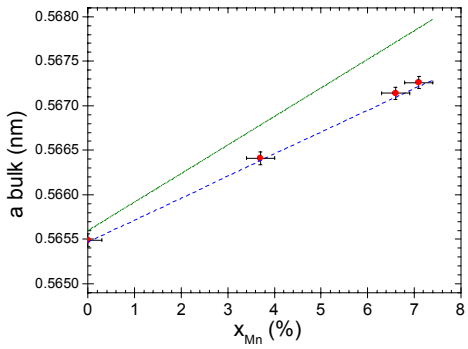

Fig. 1. Relaxed (bulk) lattice parameter of $Ga_{1-x}Mn_xAs$ *vs* composition. Our experimental points are compared to the data obtained by Ohno *et al*. [27] (in short dots) and Sadowski *et al*. [32] or Shott *et al*. [31] (same curve in dash line)

Results of X ray diffraction measurements are summarized in Table 1. The (004) reflection was analysed in an usual symmetrical geometry $\theta - 2\theta$ and the (444) reflection in an asymmetrical geometry $\omega - 2\theta$ ($\omega = \theta - \psi$ with θ the Bragg angle and ψ the angle between the sample surface and the (444) planes). The corresponding reticular distances allowed to calculate the lattice parameters of the $Ga_{1-x}Mn_xAs$ layers in the directions perpendicular ($a_\perp$) and parallel ($a_{//}$) to the sample surface. For all Mn compositions, $a_{//}$ is equal to the lattice parameter of the substrate (0.56533 nm) taking into account the accuracy of our apparatus ($\pm 10^{-4}$). These 1 μm thick layers are thus fully strained to the GaAs(001) substrate and undergo a compressive stress [28, 29]. From these results, we have calculated their relaxed (bulk) lattice parameter (a_0) assuming that $Ga_{1-x}Mn_xAs$ has the same elastic constants as GaAs in this Ga rich composition range [30]. Figure 1 shows a linear dependency of a_0 on

the Mn composition which is in good agreement with the previous works of Shott *et al.* (MBE growth at 220°C [31]) and Sadowski *et al.* (MBE at 200°C or migration-enhanced epitaxy at 150°C for $8\% \leq x \leq 10\%$ [32]). However, this behaviour is quite different to the one observed by Ohno *et al.* (MBE at 250°C [27]) but it was shown to depend strongly on the growth conditions determining the As excess incorporation [28, 31].

Samples exhibit similar magnetic and transport properties than those already reported by Ohno *et al.* [33] leading to a qualitative agreement with the phase diagram proposed. Figure 2a shows the variation of the magnetic moment as a function of temperature (T) corresponding to 3 different concentrations whereas Fig. 2b displays the variation of their conductivity. This last figure clearly illustrates the metal-insulating transition occurring when Mn concentration reaches 4.8%. At low concentration ($x < \sim 4\%$), an exponential variation of the magnetization *vs*. T can be observed thus illustrating a weak ferromagnetism phase. This low concentration limit is also characterized by an insulating phase (Fig. 2b) by which a variation of 6 orders of magnitude on the resistivity is observed when cooling down the sample from room temperature to 4K. This phase displays a low Curie temperature (about 35 K) whose behavior may be attributed to polaron percolation [34]. At higher concentration, the metallic phase is

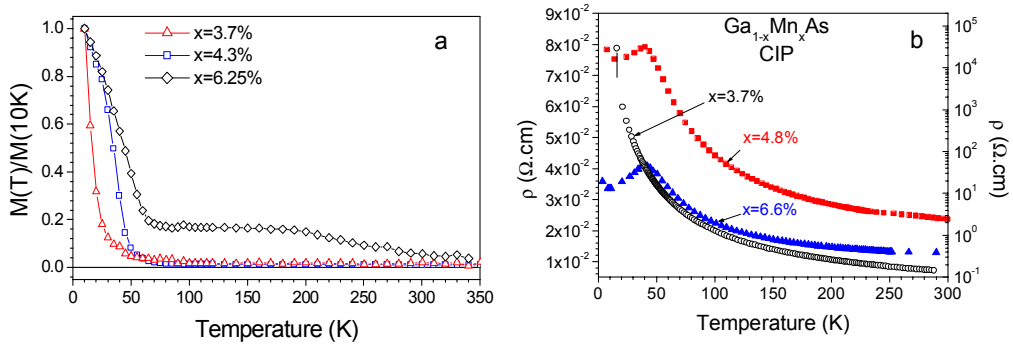

Fig. 2. a – Normalized magnetization of 1µm $Ga_{1-x}Mn_xAs$ layer with x = 3.7 (triangle), 4.3 (square), 6.25 (diamond) % as a function of the temperature; b – Resistivity as a function of the temperature for three 1 µm thick layers of $Ga_{1-x}Mn_xAs$ with x = 3.7% (open circle), 4.8% (square), 6.6% (triangle). Note that the scale for the lower concentration is on the right

achieved correspondingly to a Curie temperature larger than 60 K. With our growth conditions, the limit of solubility is reached for a concentration $x > 6.25\%$ above which the formation of MnAs cluster occurs. This effect can be evidenced on Fig. 2a where, for the highest Mn concentration, a magnetic phase persists until the room temperature corresponding to the presence of MnAs compound (T_c = 340 K).

3.2. GaMnAs/AlAs/GaMnAs tunnel junctions

To probe the spin-polarization of holes tunneling from GaMnAs through AlAs, test experiments have been performed on GaMnAs/AlAs (1.7 nm)/GaMnAs single tunnel junctions. Structures have been deposited at 230°C on a GaAs buffer layer grown at 580°C.

Junctions with diameter from 10 µm to 300 µm were patterned by optical lithography. Different thicknesses and Mn concentrations have been chosen for the two electrodes in order to obtain different coercive fields together with an antiparallel magnetic configuration. The bottom and top $Ga_{1-x}Mn_xAs$ films have respective thicknesses of 300 nm and 30 nm. The Mn concentration is 4.7% and 5.4% (bottom and top electrodes) for the single barrier. Thin layers of 1nm GaAs layer have been inserted at each side of AlAs to prevent Mn diffusion into the barrier. $M(H)$ hysteresis loops of the stack measured before patterning show two steps associated to a separate reversal of the two GaMnAs layers. The remanent magnetization, which is about 30% of the saturated magnetization reached at about 1 Tesla, collapses near 50 K. Higher Curie temperatures than 50 K have been obtained after a thermal treatment of $Ga_{0.95}Mn_{0.05}As$. Nevertheless, we have not annealed our junctions to avoid possible Mn diffusion. Figure 3a displays the tunnel magnetoresistance (TMR) measured at low bias (1 mV) and low T (4.2 K). The TMR of our single junctions, that is a probe of hole spin-polarization, is nearly as high (38%) as for the junctions of Ref. [13] with the same AlAs thickness. Using the simple Jullière formula, TMR = $2P^2/(1 - P^2)$, a tunnel polarization of 40% for holes can be deduced from these experiments even if its microscopic understanding

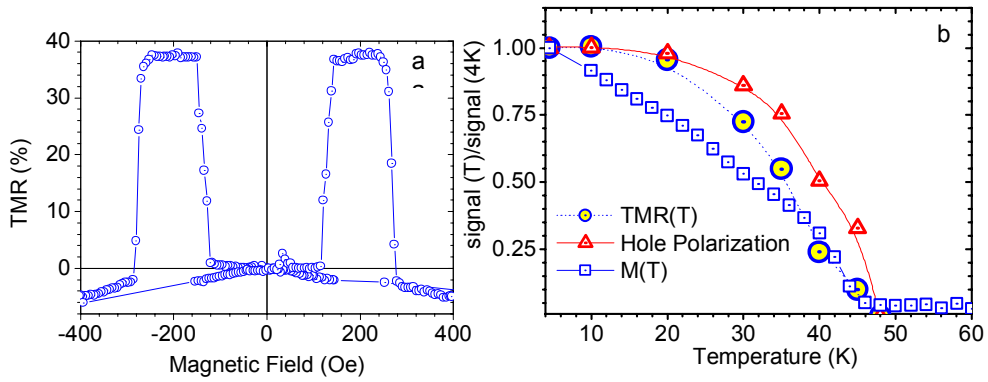

Fig. 3. a – Variation of the tunneling magnetoresistance as a function of the applied magnetic field for a GaMnAs(30nm)/AlAs(1.7 nm)/GaMnAs(300 nm) junction. TMR is defined as $100\{R(H) - R(0)\}/R(0)$; b – Variation of the normalized magnetization, the TMR and the holes polarization as a function of temperature. The holes polarization is obtained from the Julliere expression TMR = $2P^2/(1 - P^2)$

still remains a difficult task [35]. Figure 3b compares the variation of the hole tunnel polarization *vs*. T deduced from our transport measurement to the one of the magnetization obtained by SQUID magnetometer before patterning. Although both quantities cancel at the GaMnAs Curie temperature, the characteristic shape are clearly different, the hole polarization saturating at higher T. Such a different magnetic susceptibility between holes and localized d moments Mn can be explained by a stronger effective field experienced by the holes [36]. Nevertheless, microscopic calculations of the spin-polarized tunneling in GaMnAs/AlAs/GaMnAs structures are strongly required to achieve definite conclusion.

3.3. GaMnAs/AlAs/GaAs/AlAs/GaMnAs double tunnel junctions

We are now going to focus on the problem of the electrical spin detection. As largely developed in part I, the occurrence of TMR on double tunnel junctions is the signature of a spin accumulation in the central SC layer and, in that sense, can constitute such an electrical spin detection. To illustrate this idea, we have grown double tunnel junctions still constituted of two GaMnAs electrodes and where a thin GaAs layer (3, 5, 6 and 9 nm) has been inserted in between two AlAs barriers leading to GaMnAs/AlAs/GaAs/AlAs/GaMnAs structures.

The thickness of the AlAs barrier lies between 1.46 to 1.95 nm and the Mn concentration is 4.3% and 5.3% for both the bottom and top electrodes. On the other hand, Auger nanoscale spectroscopy has confirmed that the intercalation of a thin 1nm GaAs layer between GaMnAs and AlAs was sufficient to prevent any Mn diffusion into the GaAs QWs (Mn concentration less than 0.1%). A large TMR effect of about 40% is observed at low T (Fig. 4a). As described in Ref. [37], the TMR of our double junctions cannot be explained by a direct coherent tunneling between the GaMnAs electrodes but must be described by sequential tunneling with spin conservation in the GaAs QWs. This has to be associated to the half of the TMR of single junction with 1.46 nm AlAs barrier from Ref. [13]. On Fig. 4b, we have reported the TMR recorded at 4 K on different 6 nm QWs as a function of their resistance-area product RA. The resistance variation is attributed to the fluctuation of the barrier thickness from 1.46 to 1.95 nm (that is a roughness of one atomic parameter around the 1.7 nm nominal average value) like evidenced by Transmission Electronic Microscopy (TEM) cross-sections. What we observe is a continuous decrease of TMR *vs*. RA related to the reduction of the tunnel transmission. As fitted by the dot line in Fig. 4b, this behavior must be ascribed to the rise of the particle dwell time τ_n in GaAs beyond its spin lifetime τ_{sf} in GaAs for the largest barrier thickness.

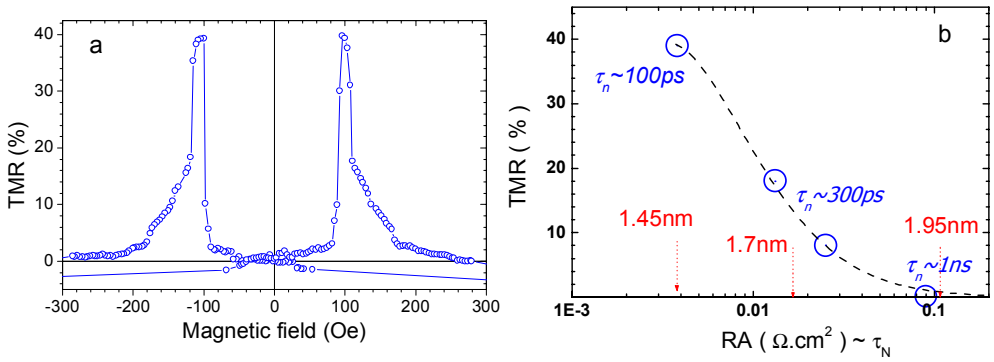

Fig. 4. a – Variation of the tunneling magnetoresistance as a function of the applied magnetic field for a GaMnAs(30 nm)/AlAs(1.45 nm)/GaAs(5 nm)/AlAs(1.45 nm)/GaMnAs(300 nm) junction; b – Variation of the TMR at 4.2 K as a function of the RA product for a GaMnAs(30 nm)/AlAs(x)/GaAs(6.2 nm)/AlAs(x)/GaMnAs(300 nm) junctions. The reported thickness x of the AlAs barriers are estimated from the RA product

From Eq. 6 and $\tau_n = (\tau_+ + \tau_-)/4$, one can evaluate τ_{sf} (at 4 K) at the value of τ_n that gives 1/3 of the maximum TMR (Fig. 4b). A rough estimation of $\tau_n \approx n\pi\hbar/(\varepsilon_n T_*)$ requires the knowledge of the barrier transparency (T_*) of GaMnAs/AlAs together with the quantized kinetic energy (ε_n) within the GaAs QWs. The latter expression of τ_n can be established by linking the 1-D DOS ρ_{SC} to ε_n and to its rank n according to $\rho_{SC} \approx n/(4\varepsilon_n)$ (*n −1 is the number of nodes of the wave function ϕ_{SC}*). In the case of extended states, ε_n can be extracted once the spatial extension of the light hole envelope function ϕ_{SC} [38] in GaAs is known (evaluated at 3-4 nm from our data). This gives a characteristic energy of about 100 meV for the first level (n = 1). The transparency of the 1.7 nm barrier was measured by Tanaka *et al.* [13] and estimated to be about 3×10^{-5}. A value of τ_n of about 300 ps is then derived also giving an order of magnitude of τ_{sf} for holes our GaAs QWs.

Such a large enhancement of τ_{sf} in a *p*-type GaAs QWs from its bulk value [39], evaluated up to some 100 ps is not new and well established theoretically [40, 41]. From an experimental point of view, this feature has been highlighted at low temperature by time resolved photoluminescence in the condition of resonant pumping on the quantized HH1 level [42, 43]. However, few remarks are necessary before to conclude: i) in our experiments, because only holes are injected by comparison to optical pumping, a long spin lifetime could be facilitated by the absence of spin relaxation introduced by electron-holes exchange [44] and ii) there is no clear evidence of resonant tunneling on a QW level in our structures. Even more, and because of the low temperature growth procedure, $R(T)$ data goes more in favor of a tunneling assisted through impurities in GaAs (Ga vacancies for instance) located at about 100-200 meV from the top of the valence band. This is also supported by the studies of the valence band matching between GaMnAs and GaAs by transport [45-46] and by photoemission [47]. Such a characteristic binding energy of 100-200 meV is then compatible with the viriel theorem that stipulates an equal magnitude between binding and kinetic energy for shallow traps. In this scenario, a long spin lifetime for holes trapped around shallow impurities and whose wavefunction has a spherical or cubic symmetry [48], can be recovered by simple argument of rotational invariance [49-51].

In conclusion we have presented experiments of spin dependent hole tunneling transport by using ferromagnetic GaMnAs electrodes as injector and detector. TMR experiments have shown that a large carrier polarization in this material can be exploited for studying the physics of spin injection into semiconductors. Moreover a spin-dependent transport through semiconductor QWs has been demonstrated. Results are understood as sequential events of spin injection, spin transport in the well before electrical detection by the counter electrode. An expression giving the level of TMR *vs.* the spin and carrier lifetimes in the QWs have been derived and probed by varying the dwell time in the well through the level of the tunnel resistance.

Acknowledgements

This research was supported by a French program Action concertée Nanosciences-Nanotechnologies and by the EU through the RTN 'Computational Magnetoelectronics' (HPRN-CT-2000-00143).

References

[1] G. Prinz, Science **282**, 1660 (1998).
[2] S. A. Wolf *et al*., Science **294**, 1488 (2001).
[3] *Semiconductor Spintronics and Quantum Computation*, Eds. D. D. Awschalom, D. Loss, and N. Samarth, Springer, Berlin (2002).
[4] A. Fert *et al*., Europhysics News **34**, vol.6 (2003).
[5] S. Datta and B. Das, Appl. Phys. Lett. **56**, 665 (1990).
[6] J. M. Kikkawa and D. D. Awschalom, Phys. Rev. Lett. **80**, 4313 (1998).
[7] R. I. Dzhioev *et al*., JETP Lett. **74** (3), 182 (2001).
[8] G. Schmidt *et al*., Phys. Rev. B **62**, 4790 (2000).
[9] E. Rashba, Phys. Rev. B **62**, R46267 (2000).
[10] A. Fert and H. Jaffrès, Phys. Rev. B **64**, 184420 (2001).
[11] T. Dietl *et al.*, Science **287**, 1019 (2000).
[12] H. Ohno, J. Magn. Magn. Mat. **200**, 110 (1999).
[13] M. Tanaka and Y. Higo, Phys. Rev. Lett. **87**, 026602 (2001).
[14] M. Tanaka and Y. Higo, Physica E **10**, 292 (2001).
[15] K. W. Edmonds *et al.*, Phys. Rev. Lett. **92**, 037201(2004).
[16] Y. Ohno *et al.*, Nature **402**, 790 (1999).
[17] R. Fiederling *et al.*, Nature **402**, 787 (1999).
[18] H. J. Zhu *et al.*, Phys. Rev. Lett. **87**, 016601 (2001).
[19] A. T. Hanbicki *et al.*, Appl. Phys. Lett. **80**, 1240 (2002).
[20] A. T. Hanbicki *et al.*, Appl. Phys. Lett. **82**, 4092 (2003).
[21] D. K. Young *et al.*, Appl. Phys. Lett. **80**, 1598 (2002).
[22] P. Van Dorpe *et al.*, Jpn. J. Appl. Phys., Part 2, **42**, L502 (2003).
[23] P. Van Dorpe *et al.*, Appl. Phys. Lett. **84**, 3495 (2004).
[24] M. Jullière, Phys. Lett. **54A**,225 (1975).
[25] R. Landauer, IBM J. Res. Develop. **1**, 223 (1957).
[26] J. Bardeen, Phys. Rev. Lett. **6**, 57 (1961).
[27] H. Ohno *et al*., Appl. Phys. Lett. **69**, 363 (1996).
[28] A. Shen *et al.*, J. Cryst. Growth **201-202**, 679 (1999).
[29] J. Sadowski *et al*., Thin Solid Films, **367**, 165 (2000).
[30] The Elastic moduli of GaAs are C_{11}=118.9 GPa ; C_{12} = 53.8 GPa whereas the strain relation for a cubic unit cell writes $(a_{\perp}-a_o)/(a_{//}-a_o) = -2.C_{12}/C_{11} = -0.905$.
[31] G. M. Shott, W. Faschinger, L. W. Molenkamp, Appl. Phys. Lett. **79**, 1807 (2001).
[32] J. Sadowski *et al.*, Appl. Phys. Lett. **78**, 3271 (2001).
[33] H. Ohno *et al.*, J. Magn. Magn. Mat. **200**, 110 (1999).
[34] A. Kaminski and S. Das Sarma, Phys. Rev. Lett. **88**, 247202 (2002).
[35] J. M. DeTeresa *et al.*, Science **286**, 507 (1999).
[36] T. Dietl *et al*. Phys. Rev. B, **63** 195205 (2001).
[37] R. Mattana et al., Phys. Rev. Lett. **90**, 166601 (2003).
[38] This is more compatible for a hole propagation direction normal to the magnetization.
[39] D. J. Hilton and C. L. Tang, Phys. Rev. Lett. **89**, 146601 (2002).
[40] R. Ferreira and G. Bastard, Phys. Rev. B **43**, 9687 (1991).
[41] R. Ferreira and G. Bastard, EuroPhys. Lett. **23**, 439 (1993).
[42] P. Roussignol *et al.*, Phys. Rev. B **46**, 7292 (1992).
[43] B. Baylac *et al.*, Solid State Com. **93**, 57 (1995).
[44] G. L. Bir, A. G. Aronov, and G. E. Pikus, Sov. Phys. JETP **42**, 705 (1976).
[45] Y. Ohno *et al.*, Physica E **13**, 521 (2002).
[46] D. Chiba, F. Matsukura, and H. Ohno, Physica E **21**, 966 (2004).
[47] H. Asklund *et al.*, Phys. Rev. B **66**, 115319 (2002).
[48] A. M. Yakunin *et al.*, Phys. Rev. Lett. **92(21)**, 216806 (2004).
[49] N. O. Lipari and A. Baldereschi, Phys. Rev. Lett. **25(24)**, 1660 (1970).
[50] A. Baldereschi and N. O. Lipari, Phys. Rev. B **8(6)**, 2697 (1973).
[51] A. Baldereschi and N. O. Lipari, Phys. Rev. B **9(4)**, 1525 (1973).